BLIND RESTORATION OF CONFOCAL MICROSCOPY IMAGES IN PRESENCE OF A DEPTH-VARIANT BLUR AND POISSON NOISE

Saima Ben Hadj [1*] , *Laure Blanc-Féraud* [1], *Gilles Aubert* [2] *and Gilbert Engler* [3]

[1] Morphème Research Group, I3S/INRIA/IBV, 06903 Sophia Antipolis, France
[2] Laboratoire J.A Dieudonne, UMR 6621 CNRS/UNSA, 06108 Nice, France
[3] IBSV Unit, INRA, 06903 Sophia Antipolis, France.

ABSTRACT

We are interested in blind image restoration in confocal laser scanning microscopy (CLSM). Two challenging problems in this imaging system are considered: First, spherical aberrations due to refractive index mismatch leads to a depth variant (DV) blur. Second, low illumination leads to a signal dependent Poisson noise. In addition, the DV point spread function (PSF) is unknown, which increases the complexity of the problem considered. Our goal is to remove in a blind framework both the DV blur and the Poisson noise from CLSM images. Using an approximation of the DV PSF, we define in a Bayesian framework a criterion to be jointly minimized w.r.t. the specimen function and the PSF. We then adopt an alternate minimization scheme for the optimization problem. For each elementary minimization, we use the recently proposed scaled gradient projection (SGP) algorithm that has shown a fast convergence rate. Results are shown on simulated and real CLSM images.

***Index Terms*—** Blind restoration, confocal microscopy, depth-variant PSF, JMAP, SGP algorithm.

1. INTRODUCTION

Confocal laser scanning microscopy (CLSM) is a powerful technique for studying biological specimens in three dimensions (3D) by optical sectioning. Nevertheless, it suffers from some artifacts. First, CLSM images are affected by a depth-variant (DV) blur due to spherical aberrations induced by refractive index mismatch between the different media composing the system as well as the specimen. Second, CLSM images are corrupted with a Poisson noise due to low illumination. Because of these intrinsic optical limitations, it is essential to remove both DV blur and noise from these images by digital processing. In this context, different restoration methods assuming that the blur is known have been developed [1, 2]. Nevertheless, in practice it is difficult to obtain such a DV Point Spread Function (PSF) in spite of the existence of theoretical PSF models accounting for spherical aberrations [3, 4], because these models are dependent on some unknown acquisition parameters (e.g. the refractive index (RI) of the specimen). Therefore a blind or semi-blind restoration algorithm needs to be developed for this system.

Different methods dealing with the blind restoration problem in the case of a space-variant (SV) blur were previously developed. Most of them are carried out under the Gaussian noise assumption. For example, in [5, 6] and in [7], two different approximation models of the SV blur are proposed and then used in the blind estimation by minimizing a quadratic criterion arising from the maximum likelihood. These two models are discussed and compared in [8, 9]. In [10], a more accurate SV PSF model is used where the PSF intensities are estimated at every pixel of the image. Although accurate, this method is prohibitive because of its huge computational cost. Some other methods dealing with the DV blind restoration problem were proposed in the literature. They essentially differ in the way of regularizing the SV PSF and the image in order to reduce the ill-posedness of the problem. We refer the reader to a few of these methods [11, 12, 13]. Nevertheless, none of these methods consider the Poisson noise case.

In this article, we propose a new DV blind restoration accounting for the Poisson noise in CLSM. Our first novel contribution w.r.t. the previous work consists in designing an appropriate constrained criterion to be minimized for the ill-posed blind restoration problem while accounting for both of the DV blur and the Poisson noise. In our proposed criterion, we combine l_1 and l_2 norms for respectively regularizing the image and the PSF. Furthermore, we consider an approximation of the DV PSF by a convex combination of a set of SI ones, as it is suggested in [8, 9]. In contrast to some existing methods [12], we do not consider any parametrization of the PSF. The non-parametric intensities of each PSF $h(x, y, z)$ are estimated for all (x, y, z). This leads to a high number of parameters to be estimated but allows more freedom on the PSF, namely on the PSF shape since it could be more or less deformed according to the spherical aberration level. Our second contribution consists in designing a fast algorithm for minimizing the proposed multivariate criterion. We propose

* Thanks to ANR Diamond for funding, R. Cavicchioli for SGP code and P. Pankajakshan for CLSM PSF code.

to use the recently published scaled gradient projection (SGP) method [14] embedded in an alternate minimization scheme. In fact, SGP method has shown a fast convergence rate w.r.t. classical gradient search methods. We denote this method by SGPAM for SGP Alternate Minimization. Furthermore, positivity constraint of the PSF and the image, PSF normalization and flux conservation are easily included thanks to the definition of SGP algorithm. This article is organized as follows: In section 2 , we give a mathematical formulation of the considered problem and define the criterion to be minimized. In section 3, we present the proposed SGPAM solver. In section 4, we present and discuss some experimental tests obtained on simulated and real CLSM images. In section 5, we conclude with a summary and some future works.

2. PROBLEM DEFINITION

Denote by $f \in \mathcal{L}^1(\mathcal{I}, \mathbb{R}^+)$ the original 3D images, with $\mathcal{I} \subset \mathbb{R}^3$ its support. Each voxel j of the recorded discrete 3D image g represents the number of photons reaching the sensor in an elementary volume $V_j \subset \mathcal{I}$. The process of photon counting follows a Poisson statistic: $g(j) \sim \mathcal{P}\left(\int_{V_j} \widetilde{H}(f)(u)\mathrm{d}u + b_g\right)$ where $u \in \mathcal{I}$ are the continuous 3D coordinates, $j \in \mathcal{I}_d \subset \mathbb{N}^3$ are the discrete 3D coordinates, and $b_g > 0$ is a constant modeling the background noise, coming from specimen auto-fluorescence or light scattering. This constant is considered to be known since it can be estimated from a region of the observed image which does not contain the specimen. $\widetilde{H}$ is the DV blur operator modeled by a convex combination of M SI PSFs taken at different depths h^i,, $i = 1, ..., M$ as: $\widetilde{H}(f) = \sum_{1 \le i \le M} h^i * (\psi^i.f)$ with $\psi^i : \mathbb{R}^3 \to [0, 1]$, $1 \le i \le M$ a set of weighting functions such that $\sum_{1 \le i \le M} \psi^i(u) = 1, \forall u \in \mathbb{R}^3$. Such a DV PSF model has been proposed in [1] and justified in [9, 8]. As we consider PSF variation only in the depth direction (z), $\psi^i(x, y, z)$ are constant along (X, Y) and linearly varying along Z-axis as given by Fig. 1. That is, each ψ^i linearly decreases when going away from the axial position of the corresponding SI PSF. Such a choice of weighting functions was shown to give comparable restoration result to that obtained by a more advanced functions predicted by principle component analysis [15]. Following a Joint Maximum A posteriori (JMAP) approach, we propose to estimate the image and the PSFs by minimizing the following criterion:

$$
\begin{aligned}
J\left(f, h^1, ..., h^M\right) = \sum_{j \in \mathcal{I}_d} \int_{V_j} \widetilde{H}(f)(u)\mathrm{d}u + b_g \\
- g(j) log \left(\int_{V_j} \widetilde{H}(f)(u)\mathrm{d}u + b_g \right) \quad (1) \\
+ \alpha \int_{\mathcal{I}} |Df| + \sum_{1 \le i \le M} \beta^i \left\|\nabla h^i\right\|_2^2
\end{aligned}
$$

The two first terms correspond to the data fidelity component related to anti-logarithm of the likelihood in the case of the Poisson statistic. The third term is the total variation function for smoothing the recovered image while preserving sharp edges. The last term is a PSF regularization term for penalizing narrow PSF. In fact, if the PSF is too narrow, a portion of the blur could be associated with the recovered image. α and β^i, $1 \le i \le M$ are regularizing parameters. In addition, we take into account other constraints: On the one hand, positivity, normalization, and bounded support constraints are imposed on the PSFs. On the other hand, positivity and flux conservation constraints are imposed on the image. For that, let denote respectively by

$$
{C_f}^c = \{f \in \mathcal{L}^1\left(\mathcal{I}, \mathbb{R}^+\right); f \ge 0; \|f\|_1 = c\}, \quad (2)
$$

$$
C_h = \{h \in \mathcal{L}^1\left(\mathcal{I}, \mathbb{R}^+\right); h \ge 0; \|h\|_1 = 1; supp\,(h) \subset B\} \quad (3)
$$

the sets of admissible image and PSF functions, where $c = \|g - b_g\|_1$ is a positive constant referring to the image flux, $supp\,(h)$ stands for the support of the PSF h and B is a given index set corresponding to a predefined PSF support. The problem that we are interested in is the following:

$$
\left(\hat{f}, \hat{h^1}, ..., \hat{h^M}\right) = \underset{C_f \times C_h^M}{arg\,min}\, J\left(f, h^1, ..., h^M\right) \quad (4)
$$

It is easy to verify that the functional $J(.)$ is convex w.r.t. each of the variables $\left(f, h^1, ..., h^M\right)$ separately (fixing the others) but globally non-convex. However, we have shown that a global minimiser of (1) exists (see [16]). As we use a deterministic method based on a gradient search technique for the minimization, the computation of a global minimum is not guaranteed and the obtained solution depend on the initialization. Theoretical PSF model [4] gives us a good initialization by approximately setting its parameters (i.e. the refractive index of the specimen is between 1 and 1.6 and the PSF depths are limited by the sample thickness).

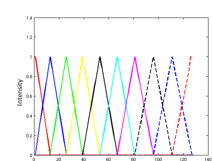

Fig. 1. Variations of 10 weighting functions ψ^i along the Z axis. They are assumed to be invariant along (X, Y).

3. PROPOSED SOLVER: SGPAM

3.1. Alternate minimization scheme

In order to solve problem (4), we propose to use an iterative alternate minimization scheme. The minimization problem is split into many steps. At each step, one variable is optimized and the others are fixed to their previous estimates:

$$\hat{f}^{(k+1)} = \underset{f \in C_f}{arg\,min}\, J\left(f,\, \hat{h^1}^{(k)},\, ...,\, \hat{h^M}^{(k)}\right) \tag{5}$$

$$\hat{h^1}^{(k+1)} = \underset{h^1 \in C_h}{arg\,min}\, J\left(\hat{f}^{(k+1)},\, h^1,\, ...,\, \hat{h^M}^{(k)}\right) \tag{6_1}$$

$$\vdots$$

$$\hat{h^M}^{(k+1)} = \underset{h^M \in C_h}{arg\,min}\, J\left(\hat{f}^{(k+1)},\, \hat{h^1}^{(k+1)},\, ...,\, h^M\right) \tag{6_M}$$

k being the iteration counter. To solve each of the above problems, we use a fast SGP algorithm [17] since the criterion is convex w.r.t. each of the variables separately. Such an algorithm was firstly applied to image deblurring [17] without regularization, then to image denoising [14] with total variation regularization. In both cases, the objective function to be minimized is different from that we consider in this article. We show in the following sub-section the main idea of SGP algorithm and how it can be applied to our problem.

3.2. SGP for image and PSF estimations

SGP [17] is proposed to solve convex constrained optimization problems of the following form: $\min_{\boldsymbol{x} \in C} \boldsymbol{J}(\boldsymbol{x})$ where $\boldsymbol{x} = (x_1, ..., x_N)^T \in \mathbb{R}^N$ is an N-dimensional vector, $C \subset \mathbb{R}^N$ is a closed convex set describing the constraints on $\boldsymbol{x}$, and $\boldsymbol{J} : C \to \mathbb{R}$ is a differentiable convex function. SGP finds a solution of that problem by approximating the following fixed point: $\boldsymbol{x}^* = P_C\left(\boldsymbol{x}^* - \delta S \nabla \boldsymbol{J}(\boldsymbol{x}^*)\right)$ where δ is a positive scalar referring to the step-length of the descent method, S is a symmetric positive definite $N \times N$ matrix which is called scaling matrix, and P_C is the projection onto C. (δS) allows to approximate the inverse of the Hessian matrix of $\boldsymbol{J}$ in order to enforce quasi-Newton properties and thus provides good convergence rate. By following the same strategy as in [14] for selecting δ and S, the SGP algorithm can be applied for solving each of problems (5), $(6)_i$, $i = 1, ..., M$. For that, we consider the following discrete notations: $\boldsymbol{f}, \boldsymbol{g}, \boldsymbol{h}^i \in \mathbb{R}^N$ are N-dimensional vectors respectively corresponding to the original image, the degraded image, and the PSFs, with N the image size. The circular convolution can be computed by the two following possible matrix-vector multiplications: $H\boldsymbol{f}$ with H an $N \times N$ matrix constructed from the SI PSF vector $\boldsymbol{h}$ or $F\boldsymbol{h}$ with F an $N \times N$ matrix constructed from the image vector $\boldsymbol{f}$. For the image estimation step (problem (5)), the function to be minimized is ($|V_j| = 1, \forall j \in \mathcal{I}_d$ in equation (1)): $\boldsymbol{J}_0(\boldsymbol{f}) = \boldsymbol{1}^T\left(\sum_{1 \le i \le M} H^i \psi^i \boldsymbol{f} + \boldsymbol{b_g}\right) - \boldsymbol{g}^T log\left(\sum_{1 \le i \le M} H^i \psi^i \boldsymbol{f} + \boldsymbol{b_g}\right) + \alpha\, \|\nabla \boldsymbol{f}\|_1$, where $\boldsymbol{1} \in \mathbb{R}^N$ is an N-size vector whose components are all equal to 1, $\boldsymbol{b_g} \in \mathbb{R}^N$ is a constant vector, $H^i \in \mathbb{R}^{N \times N}$ are matrices associated with the SI PSF $\boldsymbol{h}^i$, and $\psi^i \in \mathbb{R}^{N \times N}$ are diagonal matrices referring to weighting coefficients. Following the same steps as in [14], we derive the following expression of the matrix $S^{(n)}$ at the iteration n of SGP: $S^{(k)} = diag\left({Z^{(n)}}^{-1} \boldsymbol{f}^{(n)}\right)$ with $Z^{(n)} = diag\left(\boldsymbol{1} + \alpha V_0^R\left(\boldsymbol{f}^{(n)}\right)\right)$, $V_0^R\left(\boldsymbol{f}^{(n)}\right)$ being the positive part of the gradient of the regularization component. It can be chosen as equation (25) in [14]. Similarly, to estimate the PSFs $\boldsymbol{h}^j, j = 1, ..., M$, the following objective function is to be minimized: $\boldsymbol{J}_j\left(\boldsymbol{h}^j\right) = \boldsymbol{1}^T\left(\sum_{1 \le i \le M} F^i \boldsymbol{h}^i + \boldsymbol{b_g}\right) - \boldsymbol{g}^T log\left(\sum_{1 \le i \le M} F^i \boldsymbol{h}^i + \boldsymbol{b_g}\right) + \beta^j \left\|\nabla \boldsymbol{h}^j\right\|_2^2$ with F^i the matrix associated with the vector $\psi^i \boldsymbol{f}$. We can prove that an appropriate selection of the scaling matrix is as follows: $S^{(n)} = diag\left({E^{(n)}}^{-1} {\boldsymbol{h}^j}^{(n)}\right)$ with $E^{(n)} = diag\left(F^j \boldsymbol{1} + \beta^j V_j^R\left({\boldsymbol{h}^j}^{(n)}\right)\right)$, n being the SGP iteration number and $V_j^R\left({\boldsymbol{h}^j}^{(n)}\right)$ the positive part of the gradient of the regularization component. Note that upper and lower bounds of these scaling matrices should be adjusted according equation (26) of [14]. Moreover, using these expressions, one can update the step-length δ from Barzilai and Borwein rules given by equations (29) and (30) in [17]. Thanks to this choice of δ and S, one uses the largest possible descent step-length that decreases the energy function. Hence, the sequence $\left(J\left(\hat{f}^{(k)},\, \hat{h^1}^{(k)},\, ...,\, \hat{h^M}^{(k)}\right)\right)_{k \in \mathbb{N}}$ is decreasing and bounded below, so it is convergent.

4. EXPERIMENTAL TESTS

We present here some numerical results on simulated and real CLSM data. To assess the accuracy of our restoration result w.r.t. the reference image, we use the relative reconstruction error (RRE) and the structural similarity index (SSIM) [18]. We also compare our SGPAM based method to an other AM based method where elementary optimization problems are solved using a Regularized Richardson-Lucy algorithm [19]. We denote this latter method by RRLAM. Regularizing parameters α and β^i depend on the PSF initialization: for spread PSFs, β^i can be set to a very low value (the regularizing PSF term is useless), while for narrow PSFs, β^i should be set to a high value. In our tests, these parameters are automatically selected for a fixed PSF initialization by optimizing a no-reference quality metric that takes into account both of non-homogeneous blur and noise [20].

4.1. Test on synthetic CLSM data

We numerically generate a 3D image of $100 \times 100 \times 100$ voxels, of three spheres. The axial slice of that image is depicted in Fig. 2 (a). We then blurred that image using a DV PSF: For each Z-section we used a different PSF generated by the theoretical PSF [4]. For that, we considered the following system setting. The microscope is assumed to be equipped with a 100X oil immersion objective lens (RI 1.5) and a numerical aperture of 1.4. The cover-slip and the imaged object have respectively a RI of 1.5 and 1.48. Dye excitation was assumed to be done with the $543\,nm$ laserline of a HeNe laser and emitted light assumed to be detected using a bandpass filter $560-600\,nm$. Radial and axial pixel sizes are respectively $50\,nm$ and $145\,nm$. After blurring the considered image, we added to it a background noise of $bg = 10^{-4}$ and a Poisson noise. The axial slice of the obtained image is presented in Fig. 2 (b). We applied to that image our SGPAM algorithm using a combination of two SI PSFs, taken at the top ($z = 0$) and at the bottom ($z = z_{max}$) of the sample. Comparison of our result (cf. Fig. 2 (c)) with that obtained by RRLAM method (cf. 2 (d)) show the relevance of our method. We also compare one of the estimated PSFs $\hat{h^2}$ using SGPAM (cf. Fig. 2 (g)) and RRLAM (cf. Fig. 2 (h)) to the true PSF and the initial PSF $\hat{h^2}^{(0)}$ respectively displayed in Fig. 2 (e) and (f). Table 1 shows that SGPAM method is faster and more accurate than RRLAM. From that table, one can also note the advantage of the proposed DV blur model w.r.t. the SI case. The computing time in the SI case is sometimes slightly greater than in DV case because the algorithm requires less number of iterations to converge in the DV case than in the SI case.

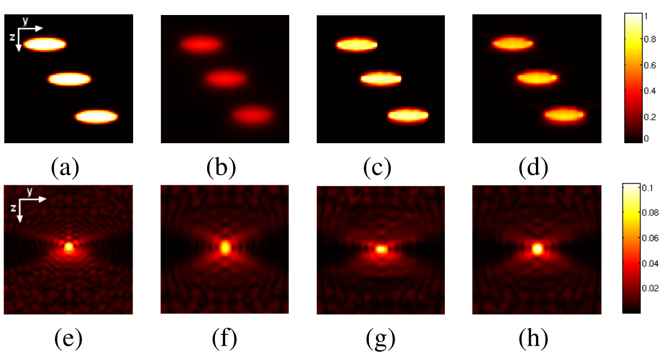

Fig. 2. $(Y,\, Z)$ slices of the obtained results on a simulated CLSM image. (a) original image, (b) simulated observation, (c) restoration using SGPAM, (d) restoration using RRLAM, (e) true PSF h^i, (f) initial PSF $\hat{h^i}^{(0)}$, (g) estimated $\hat{h^i}$ using SGPAM, and (h) estimated $\hat{h^i}$ using RRLAM for $i = 2$ ($\alpha = 10^{-3}$, $\beta^i = 0.1$, $i = 1,\, 2$).

4.2. Test on real CLSM image

Our second test is performed on a real image of a plant root of size $200 \times 200 \times 94$ voxels, observed with a Zeiss LSM 510 microscope equipped with a $40X$ oil immersion objective lens with a numerical aperture of 1.3. The radial and axial pixel-sizes are respectively $40\,nm$ and $140\,nm$. Radial and axial slices of the observed image, the restored one using a DV PSF constructed from a combination of two SI PSFs and the restored one using a SI PSF are respectively displayed in Fig. 3 (a), (b), and (c). DV blind restoration shows good results in this real image case.

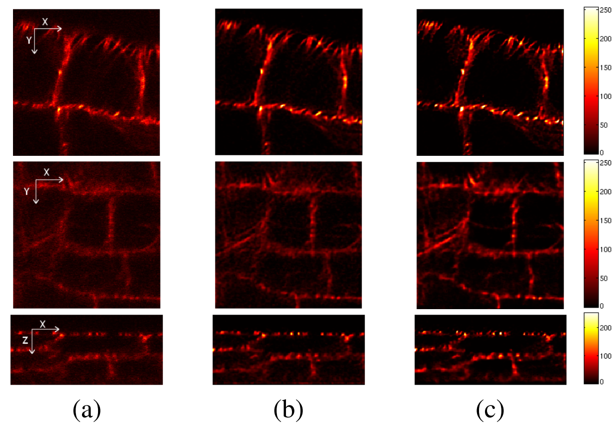

Fig. 3. $(X,\, Y)$ sections (two first lines) and $(X,\, Z)$ sections (third line) of a real CLSM image of a plant root. (a) the observation, (b) the restoration using SGPAM and a SI PSF, and (c) the restoration using SGPAM and a DV PSF ($\alpha = 0.04$, $\beta^1 = 0.01$, $\beta^2 = 10^4$).

	RRLAM		SGPAM	
	SI	DV	SI	DV
RRE (%)	20.17	16.59	16.03	7.81
SSIM	0.85	0.88	0.90	0.95
time (min)	6.90	9.10	6.7	6.18

Table 1. SGPAM method vs. RRLAM method.

5. CONCLUSION

In this article, we present a blind restoration method accounting for the DV blur and the Poisson noise in CLSM. The DV PSF is approximated by a convex combination of a set of SI PSFs. We defined a convenient criterion to simultaneously estimate the SI PSF set and the sharp image. Positivity of the unknown variables, PSF normalization, and flux conservation are ensured by the proposed SGPAM solver. Tests on simulated and real CLSM data showed the advantage of our method w.r.t. RRLAM method in terms of computational time and restoration quality. More generally, the method can be applied on any acquisition system where the PSF is space-variant and the noise follows a Poisson statistic. An interesting future work is to study the choice of the weighting functions in a blind framework. A previous study in the non-blind case can be found in [15].

6. REFERENCES

[1] C. Preza and J.A. Conchello, "Depth-variant maximum-likelihood restoration for three-dimensional fluorescence microscopy," *JOSA A*, vol. 21, no. 9, pp. 1593–1601, 2004.

[2] S. Ben Hadj and L. Blanc Féraud, "Depth-variant image restoration in 3D fluorescence microscopy: two approaches under Gaussian and Poissonian noise conditions," in *IEEE International Symposium on Biomedical Imaging (ISBI)*, Barcelone, Spain, May 2012.

[3] S.F. Gibson and F. Lanni, "Diffraction by a circular aperture as a model for three-dimensional optical microscopy," *JOSA A*, vol. 6, no. 9, pp. 1357–1367, 1989.

[4] S. F. Gibson and F. Lanni, "Experimental test of an analytical model of aberration in an oil-immersion objective lens used in three-dimensional light microscopy," *JOSA A*, vol. 8, no. 10, pp. 1601–1613, 1991.

[5] M. Hirsch, S. Sra, B. Scholkopf, and S. Harmeling, "Efficient filter flow for space-variant multiframe blind deconvolution," in *IEEE Conference on Computer Vision and Pattern Recognition (CVPR)*, 2010, pp. 607–614.

[6] S. Harmeling, M. Hirsch, and B. Schölkopf, "Space-variant single-image blind deconvolution for removing camera shake," *Advances in Neural Information Processing Systems (NIPS)*, 2010.

[7] J.G. Nagy and D.P. O'Leary, "Restoring images degraded by spatially variant blur," *SIAM Journal on Scientific Computing*, vol. 19, no. 4, pp. 1063–1082, 1998.

[8] L. Denis, E. Thiébaut, and F. Soulez, "Fast model of space-variant blurring and its application to deconvolution in astronomy," in *IEEE International Conference on Image Processing (ICIP)*, Brussels, Belgium, Sept. 2011.

[9] S. Ben Hadj and L. Blanc-Féraud, "Modeling and removing depth-variant blur from 3D fluorescence microscopy," in *IEEE International Conference on Acoustics, Speech, and Signal Processing (ICASSP)*, Kyoto, Japan, March 2012.

[10] Moritz Blume, Darko Zikic, Wolfgang Wein, and Nassir Navab, "A new and general method for blind shift-variant deconvolution of biomedical images," *Medical Image Computing and Computer-Assisted Intervention*, vol. 4791, pp. 743–750, 2007.

[11] Y.L. You and M. Kaveh, "Blind image restoration by anisotropic regularization," *IEEE Transactions on Image Processing*, vol. 8, no. 3, pp. 396–407, 1999.

[12] AN Rajagopalan and S. Chaudhuri, "MRF model-based identification of shift-variant point spread function for a class of imaging systems," *Signal processing*, vol. 76, no. 3, pp. 285–299, 1999.

[13] L. Bar, N. Sochen, and N. Kiryati, "Restoration of images with piecewise space-variant blur," *Scale Space and Variational Methods in Computer Vision*, pp. 533–544, 2007.

[14] R. Zanella, P. Boccacci, L. Zanni, and M. Bertero, "Efficient gradient projection methods for edge-preserving removal of poisson noise," *Inverse Problems*, vol. 25, pp. 045010, 2009.

[15] S. Yuan and C. Preza, "3D fluorescence microscopy imaging accounting for depth-varying point-spread functions predicted by a strata interpolation method and a principal component analysis method," in *International society for optics and photonics (SPIE)*, 2011, vol. 19, pp. 23298–23314.

[16] S. Ben Hadj, L. Blanc Féraud, and G. Aubert, "Space Variant Blind Image Restoration," Research rapport RR-8073, INRIA, Sept. 2012, http://hal.inria.fr/hal-00735135, submitted to Inverse Problems.

[17] S. Bonettini, R. Zanella, and L. Zanni, "A scaled gradient projection method for constrained image deblurring," *Inverse Problems*, vol. 25, pp. 015002, 2009.

[18] Z. Wang, A.C. Bovik, H.R. Sheikh, and E.P. Simoncelli, "Image quality assessment: From error visibility to structural similarity," *IEEE Transactions on Image Processing*, vol. 13, no. 4, pp. 600–612, 2004.

[19] N. Dey, L. Blanc-Féraud, C. Zimmer, Z. Kam, P. Roux, J.C. Olivo-Marin, and J. Zerubia, "Richardson-lucy algorithm with total variation regularization for 3d confocal microscope deconvolution," *Microscopy Research Technique*, vol. 69, no. 4, pp. 260–266, 2006.

[20] X. Zhu and P. Milanfar, "Automatic parameter selection for denoising algorithms using a no-reference measure of image content," *Image Processing, IEEE Transactions on*, vol. 19, no. 12, pp. 3116–3132, 2010.